An Analysis of Wrinkling in the Swift Cup Test

N. Triantafyllidis
Graduate Research Assistant.

A. Needleman
Associate Professor of Engineering.

Division of Engineering,
Brown University,
Providence, R.I. 02912

The onset of flange wrinkling in the Swift cup test is analyzed as a plastic bifurcation problem. The flange is modelled as an annular plate made of an orthotropic elastic-plastic material that is isotropic in the plane of the plate. The critical drawing stress and displacement obtained employing a deformation theory of plasticity and a flow theory of plasticity are compared. The effects of flange geometry and material properties on wrinkling are investigated. Employing a simple linear elastic spring model of the blankholder, the effect of blankholder stiffness on wrinkling is studied. The present results for the critical stress at the onset of wrinkling and for the number of wrinkles are compared with those obtained previously employing a beam model of the flange.

1 Introduction

Much recent activity (as witnessed by the symposia volumes [1, 2]) has been directed toward analyzing tensile instabilities in sheet forming processes. Less attention has been focussed on analysis of the compressive instabilities encountered in sheet forming operations. Here, we analyze the onset of wrinkling, a compressive bifurcation instability, in the Swift cup test, where, as sketched in Fig. 1, a circular flat sheet is drawn into a cup by a cylindrical punch. In this context the term wrinkling refers specifically to the formation of buckles (or wrinkles) in the flange, which is the portion of the sheet remaining between the die and the blankholder.

A principal objective of the Swift cup test is to determine the limiting drawing ratio (LDR), defined as the largest drawing ratio, b/a, from which a cup can be drawn without fracture. Here, b and a are the radii of the sheet and punch, respectively. For some sheet metals the LDR lies within the range between 2.0 and 2.5. Unless sufficient restraint is provided by the blankholder, wrinkling will occur for drawing ratios in this range. For smaller drawing ratios, how much smaller depending on the sheet thickness and properties, wrinkling will *not* occur even without the blankholder.

We model the flange as an annular plate subject to axisymmetric radial tension along its inner edge, as shown in Fig. 2. Frictional forces on the flange are neglected. The bifurcation problem governing the onset of wrinkling is formulated within the context of the standard small strain nonlinear plate theory employed in plate buckling analyses [3]. A numerical solution is obtained by employing separation of variables in conjunction with a finite element method.

Quite recently, Naruse and Takeyama [18, 19] have also modeled flange wrinkling as a plastic bifurcation problem for an annular plate. Aspects of their formulation and the numerical method employed in [18, 19] differ from the present approach.

The sheet material is characterized by an elastic-plastic

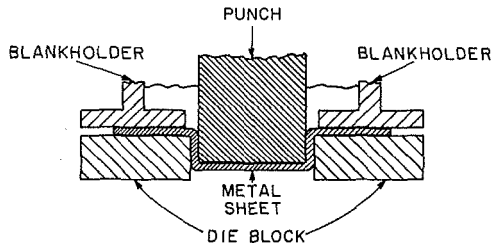

Fig. 1 Schematic of the Swift Cup Test

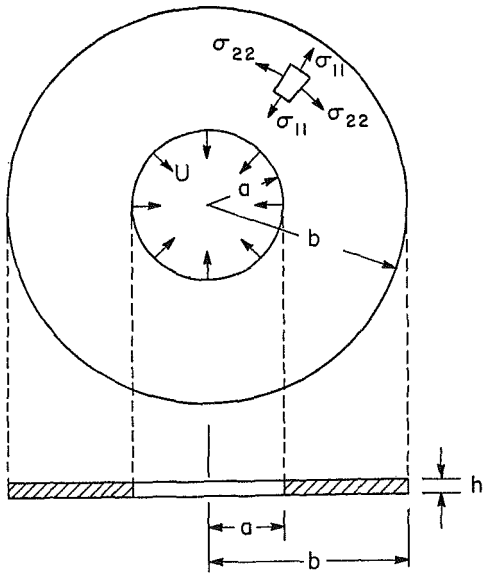

Fig. 2 The flange geometry

Contributed by the Materials Division for publication in the JOURNAL OF ENGINEERING MATERIALS AND TECHNOLOGY. Manuscript received by the Materials Division, November 13, 1979.

constitutive law which presumes isotropy (elastic and plastic) in the plane of the sheet, but normal plastic anisotropy is accounted for. Most of the numerical results are obtained employing a deformation theory of plasticity since, as has long been realized in structural mechanics applications, the classical smooth yield surface flow theories of plasticity often over-estimate the critical stress for bifurcation.

The use of a deformation theory of plasticity in a bifurcation analysis can be rigorously justified by appealing to a solid with a vertex on its yield surface at the current loading point, see e.g., [4]. Indeed, such yield surface vertices are predicted by physical theories of polycrystalline plasticity based on single crystal slip, see e.g., [5], although experimental evidence concerning the existence of yield surface vertices is ambiguous and contradictory [6].

The predictions of the deformation theory for the onset of wrinkling are compared and contrasted with the corresponding smooth yield surface flow theory predictions. The effects of flange width and thickness and material properties, in particular strain hardening and plastic anisotropy, on wrinkling are investigated. The restraint provided by the blankholder is modeled as a simple linear elastic foundation on which the flange rests. The effect of the stiffness of this foundation on retarding the onset of wrinkling and on the number of wrinkles formed is explored.

The present results, for the critical stress at the onset of wrinkling and for the number of wrinkles, are compared with those obtained by Senior [7] employing a highly approximate beam model of the flange.

2 Constitutive Relations

The present analysis is carried out within the framework of plane stress theory and the in-plane stress increments, $\dot{\sigma}_{\alpha\beta}$,[1] are taken to be related to the strain increments, $\dot{\epsilon}_{\alpha\beta}$, by a constitutive relation of the form

$$\dot{\sigma}_{\alpha\beta} = L_{\alpha\beta\gamma\delta}\dot{\epsilon}_{\gamma\delta} \tag{1}$$

where the tensor of plane stress moduli, $\mathbf{L}$ is given in terms of the 3-D moduli, $\hat{\mathbf{L}}$, by

$$L_{\alpha\beta\gamma\delta} = \hat{L}_{\alpha\beta\gamma\delta} - \frac{\hat{L}_{\alpha\beta 33}\hat{L}_{\gamma\delta 33}}{\hat{L}_{3333}} \tag{2}$$

Two constitutive laws are employed here. One is a flow theory of plasticity with a smooth yield surface, while the other is the corresponding "total" or deformation theory of plasticity. In each case the total strain increment is written as

$$\dot{\epsilon}_{ij} = \dot{\epsilon}^e_{ij} + \dot{\epsilon}^p_{ij} \tag{3}$$

The elastic response is taken to be isotropic so that

$$\dot{\epsilon}^e_{ij} = \frac{1}{E}[(1+\nu)\dot{\sigma}_{ij} - \nu\dot{\sigma}_{kk}\delta_{ij}] \tag{4}$$

where E is Young's modulus and ν is Poisson's ratio.

In the theory of anisotropic plasticity employed here, due to Hill [8, Chapt. XII], the effective stress, σ_e, is taken to be

$$\sigma_e^2 = \frac{(1+R)\sigma_{11}^2 + (1+R)\sigma_{22}^2 + 2\sigma_{33}^2 - 2R\sigma_{11}\sigma_{22} - 2\sigma_{11}\sigma_{33} - 2\sigma_{22}\sigma_{33} + 2(1+2R)\sigma_{12}^2}{(1+R)} \tag{5}$$

[1] Here, and subsequently, Greek indices range from 1 to 2, with 1 denoting the r-direction and 2 the θ-direction in a polar coordinate system. The normal direction is denoted by the index 3. Latin indices when employed subsequently will range from 1 to 3.

In (5), the dependence of the effective stress on the shear stresses σ_{13} and σ_{23} is not exhibited, since these stresses do not enter into the constitutive law within the present plane stress framework.

The parameter R measures the normal anisotropy. This parameter is defined, in a uniaxial tensile test of a sheet element, as the ratio of the width plastic strain in the plane of the sheet to the plastic strain through the thickness. For an isotropic material $R = 1$.

For flow theory, with the yield surface given by $\sigma_e = Y$, where Y is the current value of the tensile flow strength, the plastic strain increments, $\dot{\epsilon}^p_{ij}$, are given by

$$\dot{\epsilon}^{\mathrm{P}}_{\mathrm{ij}} = \left(\frac{1}{\mathrm{E}_t} - \frac{1}{\mathrm{E}}\right)\frac{\partial\sigma_e}{\partial\sigma_{ij}}\frac{\partial\sigma_e}{\partial\sigma_{kl}}\dot{\sigma}_{kl} \tag{6}$$

if $\sigma_e = Y$ and $\dot{\sigma}_e \geq 0$; otherwise $\dot{\epsilon}^P_{ij} \equiv 0$. The tangent modulus, E_t, is a function of σ_e and is the slope of the effective stress-effective strain curve.

The deformation theory of plasticity is a small strain nonlinear elastic constitutive law, which coincides with (6) for proportional loading paths. Thus, by integrating (6) for proportional loading, we obtain

$$\epsilon^P_{ij} = \left(\frac{1}{\mathrm{E}_s} - \frac{1}{\mathrm{E}}\right)\sigma_e\frac{\partial\sigma_e}{\partial\sigma_{ij}} \tag{7}$$

where E_s is the ratio of effective stress to effective strain at stress level σ_e.

Differentiating (7) with respect to some monotonically increasing loading parameter gives

$$\dot{\epsilon}^P_{ij} = \left(\frac{1}{\mathrm{E}_t} - \frac{1}{\mathrm{E}_s}\right)\frac{\partial\sigma_e}{\partial\sigma_{ij}}\frac{\partial\sigma_e}{\partial\sigma_{kl}}\dot{\sigma}_{kl} + \left(\frac{1}{\mathrm{E}_s} - \frac{1}{\mathrm{E}}\right)\sigma_e\frac{\partial^2\sigma_e}{\partial\sigma_{ij}\partial\sigma_{kl}}\dot{\sigma}_{kl} \tag{8}$$

Employing (6), for flow theory, or (8), for deformation theory, in (3) and using (4) gives the strain increments, $\dot{\epsilon}_{ij}$, in terms of the stress increments, $\dot{\sigma}_{ij}$. This relation can then be inverted to obtain the 3-D tensor of moduli $\hat{\mathbf{L}}$ given in the Appendix.

Here, it is assumed that the effective stress and effective strain are related by the piecewise power law

$$\frac{\epsilon_e}{\epsilon_y} = \begin{cases} \dfrac{\sigma_e}{\sigma_y} & \sigma_e < \sigma_y \\ \left(\dfrac{\sigma_e}{\sigma_y}\right)^m & \sigma_e \geq \sigma_y \end{cases} \tag{9}$$

where m is the hardening exponent and σ_y and ϵ_y are the uniaxial yield stress and yield strain, respectively. From (9)

$$E_t = \frac{\mathrm{E}}{m}\left(\frac{\sigma_e}{\sigma_y}\right)^{1-m} \qquad \mathrm{E}_s = \mathrm{E}\left(\frac{\sigma_e}{\sigma_y}\right)^{1-m} \qquad \sigma_e \geq \sigma_y \tag{10}$$

and $\mathrm{E}_t = \mathrm{E}_s = \mathrm{E}$ for $\sigma_e < \sigma_y$.

The tensor of moduli, $\hat{\mathbf{L}}$, for flow theory has two branches; one corresponding to plastic loading, the other to elastic unloading. In the particular problem considered here, the plastic loading condition ($\dot{\sigma}_e > 0$) is always satisfied subsequent to initial yielding. Hence the plastic loading branch is active everywhere in the current plastic zone.

The use of deformation theory in bifurcation calculations where the prebifurcation path is one of proportional or nearly proportional loading (as will be the case here) was first justified by Batdorf [9]. This justification, which provides the rationale for the use of deformation theory bifurcation formulae in structural mechanics applications, is based on the observation that for nearly proportional loading increments there exists a flow theory with a vertex on its yield surface whose instantaneous moduli coincide with those of deformation theory. In fact Sanders [10] explicitly constructed such a corner theory whose moduli in this total loading regime coincide with those of the isotropic ($R = 1$) version of (8). Very recently, Christoffersen and Hutchinson [11] have constructed a class of phenomenological vertex theories which coincide with a deformation theory for nearly proportional loading increments and give a smooth transition to elastic unloading for increasingly nonproportional increments. Hence, the deformation theory moduli employed here can be regarded as being those associated with the total loading regime of some incremental theory with a corner on its yield surface.

3 Analysis of the Onset of Wrinkling

The inner radius of the annular plate representing the flange is specified by a and the outer radius by b as depicted in Fig. 2. The thickness of the sheet is denoted by h. The plate is assumed to be thin ($h/a << 1$) and the standard Kirchhoff hypotheses of plate theory are invoked.

In the specific annular plate problem considered here the loading is taken to be applied through a monotonically increasing tensile radial displacement, U, at the plate's inner edge, while the outer edge remains stress free. One state of deformation consistent with this loading is an axisymmetric planar deformation state. In this prebifurcation state, the displacement of a point on the middle surface is specified by a radial in-plane displacement $u(r)$, where r is the distance of a point on the middle surface from the axis of symmetry.

The boundary conditions take the form

$$\dot{u}(a) = -\dot{U} \tag{11a}$$

$$\dot{\sigma}_{11}(b) = 0 \tag{11b}$$

The non-vanishing membrane strain increments are

$$\dot{e}_{11} = \dot{u}_{,r} \quad \dot{e}_{22} = \dot{u}/r \tag{12}$$

where $(\ )_{,r}$ denotes differentiation with respect to the radial coordinate, r.

By employing the relations (12) we have presumed that the prebifurcation strains are small. As will be seen subsequently, over virtually the entire range of parameters considered here, the assumption of small prebifurcation strains is indeed appropriate.

The boundary value problem governing the axisymmetric prebifurcation state can be formulated in terms of the following variational principle: Among all displacement increment fields $\dot{u}(r)$ that satisfy the kinematic boundary condition (11a), the actual field satisfies

$$\delta I = 0 \tag{13}$$

where

$$I = \pi h \int_a^b (\dot{\sigma}_{11}\dot{e}_{11} + \dot{\sigma}_{22}\dot{e}_{22}) r dr \tag{13b}$$

In (11b), the radial and hoop stress increments, $\dot{\sigma}_{11}$ and $\dot{\sigma}_{22}$, respectively, are related to the strain increments in (12) by the plane stress moduli, $\mathbf{L}$, for flow theory or deformation theory, as appropriate.

The variational principle (13) forms the basis for implementing a finite element solution for the prebifurcation state. The interval $a \le r \le b$ is divided into a number of subintervals and the displacement increment is expressed in terms of Hermitian cubic polynomials within each subinterval. The prebifurcation deformation history is then calculated in a straighforward linear incremental manner.

Bifurcation from this planar axisymmetric deformation state into a non-planar state is then considered at some stage of the deformation history. We denote by $\dot{w}$ the lateral displacement in the bifurcation mode, which is, in general, a function of the polar angle θ as well as of the radial coordinate r.

The bifurcation mode curvatures, $\dot{\kappa}_{\alpha\beta}$, are given in terms of the bifurcation mode displacement, $\dot{w}$, by

$$\dot{\kappa}_{11} = -\dot{w}_{,rr} \quad \dot{\kappa}_{22} = -\frac{1}{r}\dot{w}_{,r} - \frac{1}{r^2}\dot{w}_{,\theta\theta}$$

$$\dot{\kappa}_{12} = -\left(\frac{1}{r}\dot{w}_{,\theta}\right)_{,r} \tag{14}$$

The bifurcation mode moments $\dot{M}_{\alpha\beta}$ are related to the curvatures $\dot{\kappa}_{\alpha\beta}$ by

$$\dot{M}_{\alpha\beta} = \frac{h^3}{12} L_{\alpha\beta\gamma\delta}\ \dot{\kappa}_{\gamma\delta} \tag{15}$$

where in Hill's [12, 13] terminology $\mathbf{L}$ is the tensor of moduli associated with an appropriate linear comparison solid. The appropriate linear comparison solid moduli for flow theory correspond to the plastic loading branch being active everywhere in the current plastic zone and the tensor of elastic moduli being active in the current elastic region.

As discussed previously, the deformation theory moduli are regarded as those of the linear comparison solid associated with a flow theory with a vertex on its yield surface. Hence, the bifurcation calculations carried out here employing the deformation theory moduli in the current plastic zone are rigorously valid for some flow theory with a singular yield surface [4, 9–11]. Although the analysis here is limited to consideration of bifurcation, we note that a consideration of post-bifurcation behavior, which involves strongly nonproportional loading, would require a specification of the constitutive behavior outside the total loading regime, as for example given in [11].

We assume that no bending moment is transmitted across the die throat so that the annular plate representing the flange is simple supported at $r = a$. Thus,

$$\dot{w}(a,\theta) = 0 \quad \dot{M}_{11}(a,\theta) = 0 \tag{16}$$

The outer edge of the plate, $r = b$, is assumed to be stress free so that the shear force and bending moment vanish there, so that

$$\dot{M}_{11}(b,\theta) = 0 \quad \dot{Q}_{\text{eff}}(b,\theta) = 0 \tag{17}$$

where Q_{eff} denotes the Kirchhoff effective shear [3].

One way in which the blankholder loading may be applied is by springs or by the stiffness of the bolts holding down the blankholder plate, giving rise to a surface load which depends on the lateral displacement of the flange.

A rigorous representation of this induced surface load leads

to an eigenvalue problem in which the region of contact between the blankholder and the flange, in the buckled configuration, must be determined as part of the solution. Here, to explore the effect of the blankholder on wrinkling, we rest the annular plate on a continuous linear elastic foundation, which gives an effective surface load, $\dot{p}$, of the form

$$\dot{p}(r,\theta) = -k\dot{w}(r,\theta) \tag{18}$$

where k is the spring constant of the foundation. The elastic foundation spring constant, k, is related to the blankholder stiffness, K, by equating the elastic energies stored in the foundation and in the blankholder. Thus, since the deflection of the spring blankholder is twice the amplitude of the wrinkles,

$$k = \frac{\gamma^{-1}K}{\pi(b^2-a^2)} \qquad \gamma = \frac{\int_0^{2\pi}\int_a^b \dot{w}^2(r,\theta)rdrd\theta}{4\pi(b^2-a^2)} \tag{19}$$

where $\dot{w}(r,\theta)$ is taken to have a unit amplitude.

Under these conditions, bifurcation from the planar axisymmetric deformation state is possible when a nontrivial solution exists to the homogeneous equations

$$\delta F = 0 \tag{20a}$$

$$F = \frac{1}{2}\int_0^{2\pi}\int_a^b \left[\frac{h^3}{12}L_{\alpha\beta\gamma\delta}\dot{\kappa}_{\alpha\beta}\dot{\kappa}_{\gamma\delta} + h\sigma_{\alpha\beta}\dot{w}_{,\alpha}\dot{w}_{,\beta} + k\dot{w}^2\right] rdrd\theta = 0 \tag{20b}$$

Here, σ is the prebifurcation stress state and the linear comparison solid moduli $\mathbf{L}$ are evaluated at the stress state σ.

Any admissable bifurcation mode displacement, $\dot{w}$, in (20) must satisfy the kinematic boundary condition, $\dot{w} = 0$, at the inner edge $r = a$. Due to the requirement of periodicity, $\dot{w}$, can be expanded in a Fourier sine or cosine series of the form

$$\dot{w}(r,\theta) = W_0(r) + \sum_{n=1}^{\infty} W_n(r)\cos n\theta \tag{21}$$

Substituting (21) into (19b) and integrating with respect to θ, while exploiting the orthogonality properties of the trigonometric functions leads to the bifurcation functional F in (20b) assuming the form

$$F(w) = F_0(W_0) + \frac{1}{2}\sum_{n=1}^{\infty} F_n(W_n) \tag{22}$$

where each F_n has the form

$$F_n(W_n) = \int_a^b \left[\frac{h^3}{12}\left(L_{1111}W_{n,rr}^2 + 2L_{1122}W_{n,rr}\left(\frac{1}{r}W_{n,r} - \frac{n^2}{r^2}W_n\right) + L_{2222}\left(\frac{1}{r}W_{n,r} - \frac{n^2}{r^2}W_n\right)^2 + 4L_{1212}\left\{\left(\frac{nW_n}{r}\right),r\right\}^2\right) + h\sigma_{11}W_{n,r}^2 + h\sigma_{22}\left(\frac{nW_n}{r}\right)^2 + kW_n^2\right]rdr \tag{23}$$

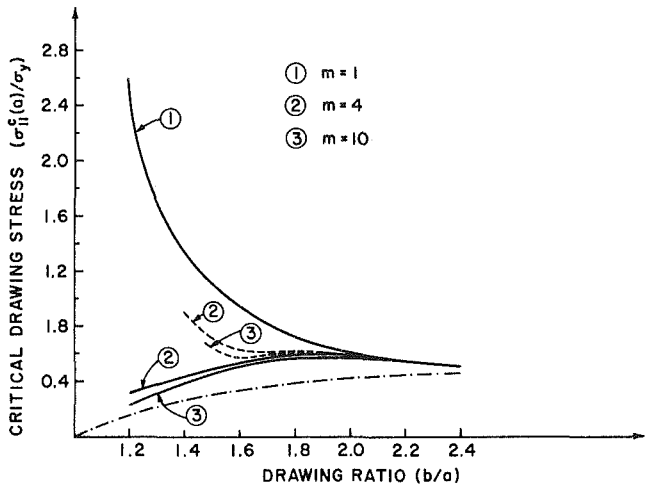

Fig. 3 Critical drawing stress, $(\sigma_{11}^c(a)/\sigma_y)$, versus the drawing ratio (b/a) for deformation theory (——) and flow theory (---) with hardening exponents, m = 1, 4, 10. For all points below the (—·—·—) curve, the entire flange is in the elastic region. Results obtained for $h^2/a^2\epsilon_y = 0.9$, $\nu = 0.3$, $R = 1$ and $K/h\sigma_y = 0$.

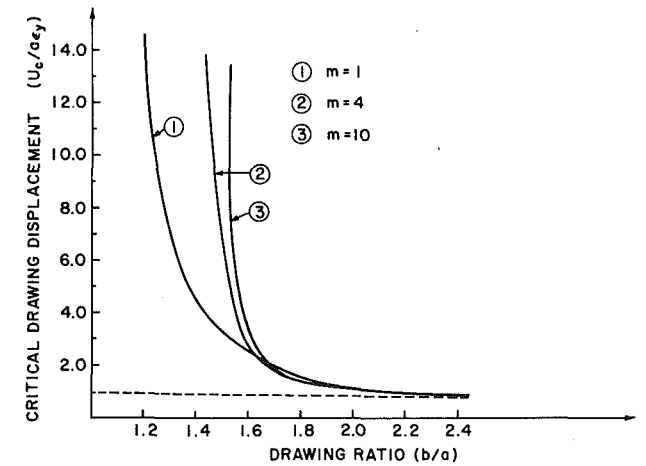

Fig. 4 Critical drawing displacement, $U_c/a\epsilon_y$, versus the drawing ratio (b/a), for flow theory with hardening exponents m = 1, 4, 10. For all points below the (———) curve the entire flange is in the elastic region. Results obtained for $h^2/a^2\epsilon_y = 0.9$, $\nu = 0.3$, $R = 1$, $K/h\sigma_y = 0$.

Bifurcation first occurs at the smallest value of the applied displacement, U, for which some F_n satisfies

$$\delta F_n(W_n) \quad F_n(W_n) = 0 \tag{24}$$

The corresponding bifurcation mode is of the form $W_n(r)\cos n\theta$ (or $W_n(r)\sin n\theta$).

The bifurcation calculation is carried out by a similar numerical procedure to that described in [14]. An increment of the prebifurcation solution is calculated as described previously. The lateral displacement $W_n(r)$ for selected values of n is then expressed in terms of Hermitian cubic polynomials within each element. The stiffness matrix associated with each $F_n(W_n)$ is assembled and when the determinant of this stiffness matrix vanishes, the current value of U is the critical one for bifurcation into the nth mode. Several checks were made on the numerical procedure. For a pure power law hardening material, that axisymmetric prebifurcation state agreed with that given by the analysis of [15]. When the loading was changed to external compression and attention confined to axisymmetric bifurcation, the results obtained by the present analysis were in agreement with those in [17].

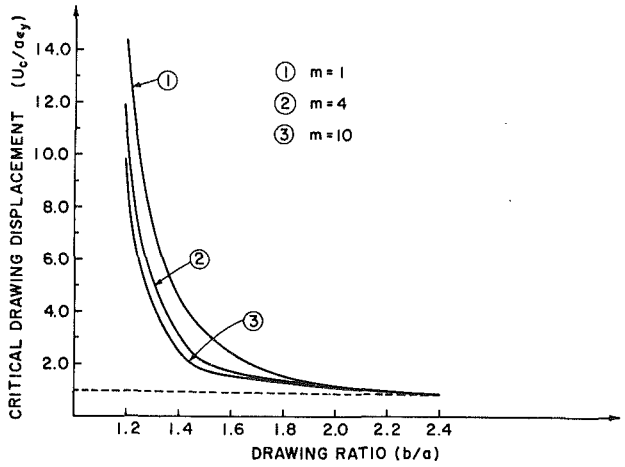

Fig. 5 Critical drawing displacement, $U_c/a\epsilon_y$, versus the drawing ratio (b/a) for deformation theory with hardening exponents $m = 1, 4, 10$. For all points below the (···) curve, the entire flange is in the elastic region. Results obtained for $h^2/a^2\epsilon_y = 0.9$, $\nu = 0.3$, $R = 1$, $K/h\sigma_y = 0$.

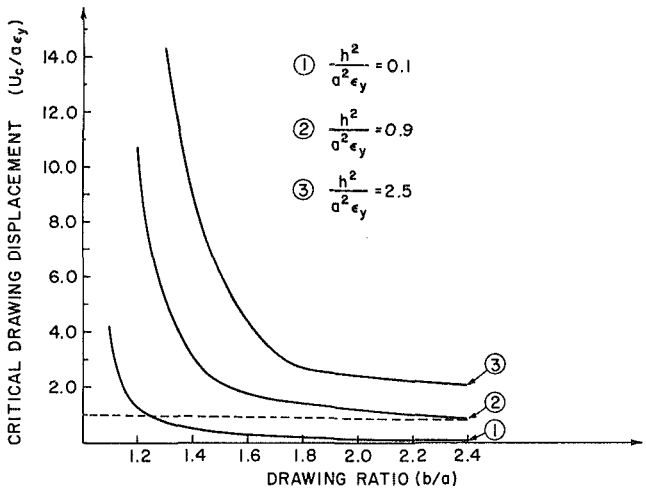

Fig. 6 Critical drawing displacement, $U_c/a\epsilon_y$, versus the drawing ratio b/a, for deformation theory with thickness parameters h^2a^2 $\epsilon_y = 0.1, 0.9, 2.5$. For all points below the (——) curve, the entire flange is in the elastic region. Results obtained for $m = 4$, $\nu = 0.3$, $R = 1$, $K/h\sigma_y = 0$.

4 Numerical Results

The critical drawing stress, $\sigma_{11}^c(a)$, for the onset of wrinkling normalized by the yield stress, σ_y, depends on the geometric and material parameters through the following dimensionless groups

$$\frac{\sigma_{11}^c(a)}{\sigma_y} = f\left(\frac{h^2}{a^2\epsilon_y}, \frac{b}{a}, m, \nu, R, \frac{K}{h\sigma_y}\right) \tag{25}$$

where h/a is the flange thickness divided by the punch radius, $\epsilon_y = \sigma_y/E$, with σ_y denoting the yield stress and E Young's modulus, b/a is the drawing ratio, m is the strain hardening exponent, υ is Poisson's ratio, R is the plastic anisotropy coefficient and K is the blankholder stiffness.

Figures 3–6 display the results obtained here for the onset of wrinkling without a blankholder ($K = 0$) as a function of the drawing ratio, b/a. In these calculations Poisson's ratio, ν, was taken as 0.3 and plastic isotropy, $R = 1$, was assumed to hold.

Figure 3 depicts the dependence of the normalized critical drawing stress, $\sigma_{11}^c(a)/\sigma_y$, on the strain hardening exponent, m, of the flange material. The normalized flange thickness, $h^2/a^2\epsilon_y$, is taken to be 0.9, corresponding to a flange thickness to punch radius ratio, h/a, of 0.03 if $\epsilon_y = 0.001$, or if $\epsilon_y = 0.004$ then $h^2/a^2\epsilon_y = 0.9$ corresponds to $h/a = 0.06$. Results are shown for two values of m; $m = 4$, corresponding to a moderately hardening material and $m = 10$ corresponding to a lightly hardening material. For comparison purposes results are also displayed for a linear elastic material, $m = 1$.

The dashed curves in Fig. 3 are the flow theory predictions, while the solid curves are the corresponding deformation theory results. Of course, for $m = 1$ the two theories coincide. For drawing ratios greater than about 1.8 most of the flange is in the elastic regime and, due to this elastic restraint, the critical drawing stress differs little from that for a linear elastic material for drawing ratios in this range.

Except for the linear elastic material, none of the curves in Fig. 3 exhibits a monotonic depenence of the critical drawing stress on the drawing ratio. For drawing ratios less than 1.6, the deformation theory predicts a decreasing drawing stress with decreasing drawing ratio while the critical drawing stress obtained from flow theory increases. The flow theory curves in Fig. 3 are terminated before the deformation theory curves since the strains in the flange at the predicted onset of wrinkling, according to flow theory, rise very steeply beyond the depicted range.

If as in [15] we assume that the punch load, P_c, is related to the drawing stress $\sigma_{11}^c(a)$ by

$$P_c = 2\pi a(1+\eta)h\sigma_{11}^c(a) \tag{26}$$

where η is an empirical constant intended to incorporate the effect of friction at the die throat, then Fig. 3 implies that according to deformation theory, the punch load at the onset of wrinkling decreases with the drawing ratio for drawing ratios less than about 1.6. On the other hand, flow theory predicts an increasing critical punch load for wrinkling in this regime. Assuming (26) holds, neither theory predicts a monotonic dependence of the critical punch load for wrinkling on the drawing ratio. Figures 4 and 5 show the results of the same calculations as depicted in Fig. 3. However, in Figs. 4 and 5 the critical radial displacement, U_c, for the onset of wrinkling is plotted as a function of the drawing ratio, b/a. The radial displacement is normalized by the punch radius, a, and the yield strain, ϵ_y, with the quantity $U_c/a\epsilon_y$ representing critical hoop strain at the die throat divided by the yield strain.

Figure 4 displays the results for flow theory while Fig. 5 displays the corresponding results for deformation theory. Note that in each figure the critical displacement for the onset of wrinkling increases monotonically as the drawing ratio decreases. According to flow theory the value of $U_c/\epsilon_y a$ is higher for a lightly hardening material, $m = 10$, than for a moderately hardening material, $m = 4$, except for the larger drawing ratios where the role of plasticity is not significant. On the other hand, deformation theory predicts an increasing critical die throat displacment, U_c, as strain hardening capacity increases.

Figure 6 illustrates the effect of flange thickness on wrinkling. Here, deformation theory was employed with a strain hardening exponent, m, of 4. For a thin flange, $h^2/a^2\epsilon_y = 0.1$, wrinkling initiates prior to plastic yielding over most of the range of interest.

The calculations with a blankholder present, displayed in Tables 1 and 2, were carried out for fixed values of γ^{-1} $K/h\sigma_y$. In Table 1, the values $\gamma^{-1}K/h\sigma_y = 100$ and 500 were employed, while in Table 2 $\gamma^{-1}K/h\sigma_y = 100$ and 1000. The quantity γ was calculated for selected cases and these values of γ employed to obtain the values of $K/h\sigma_y$, rounded to an integer, listed in the tables. The values of γ obtained did not depend significantly on the drawing ratio. For example, γ^{-1} $K/h\sigma_y = 500$ and $b/a = 2.0$ gave a value of $\gamma = 0.035$ while

Table 1 The effect of the blankholder stiffness on wrinkling, for deformation theory with $h^2/a^2\epsilon_y = 0.1$, $R = 1$, $\nu = 0.3$, $m = 4$

$\frac{K}{h\sigma_y}$	$\frac{b}{a}$	$\frac{\sigma_{11}^c(a)}{\sigma_y}$	$\frac{U_c}{a\,\epsilon_y}$	n
0	2.0	0.07	0.13	3
0	1.6	0.11	0.28	4
0	1.2	0.20	1.24	5
6	2.0	0.69	1.59	10
6	1.6	0.52	1.58	11
6	1.2	0.24	2.49	16
17	2.0	0.92	3.09	19
17	1.6	0.63	2.96	21
17	1.2	0.29	6.27	27

Table 2 The effect of the transverse anisotropy ratio R on wrinkling, for deformation theory with $h^2/a^2\epsilon_y = 0.9$, $b/a = 1.6$, $\nu = 0.3$, $m = 4$

$\frac{K}{h\sigma_y}$	R	$\frac{\sigma_{11}^c(a)}{\sigma_y}$	$\frac{U_c}{a\,\epsilon_y}$	n
0	0.5	0.58	1.85	4
0	1.0	0.55	1.78	4
0	2.0	0.54	1.85	4
0	4.0	0.53	1.81	4
4	0.5	0.75	5.26	9
4	1.0	0.75	6.09	9
4	2.0	0.75	7.16	9
4	4.0	0.75	8.16	9
24	0.5	1.11	26.59	22
24	1.0	1.14	34.89	22
24	2.0	1.18	45.92	21
24	4.0	1.20	56.08	21

for $b/a = 1.2$, $\gamma = 0.033$. Furthermore, it was found that the bifurcation mode deflection $\dot{w}(r)$ increased monotonically from $r = a$ to $r = b$, as expected, for the cases with $b/a = 2.0$ or less. For a larger drawing ratio, $b/a = 2.4$, radial oscillations in the deflections pattern were obtained, which was taken to indicate that the linear elastic foundation model of the blankholder was not appropriate for such a large drawing ratio.

Table 1 illustrates the effect of the blankholder stiffness on wrinkling behavior. These results were obtained using the deformation theory, with the flange thickness and material properties taken as shown in the table. In addition to considerably delaying the onset of wrikling, the blankholder stiffness greatly increases the number of wrinkles. For example, for $b/a = 1.6$, without a blankholder wrinkling initiates at $U_c/a\epsilon_y = 1.24$ with 5 wrinkles. With a nondimensional blankholder stiffness of 17, for $b/a = 1.6$, the number of wrinkles is increased to 21 and $U_c/a\epsilon_y = 6.27$.

Table 2 illustrates the effect of the normal anisotropy parameter, R, on wrinkling. These results also employ the deformation theory and are for $b/a = 1.6$. In the absence of the blankholder, $K = 0$, $U_c/a\epsilon_y$ is virtually independent of R. With a blankholder present, the critical displacement for wrinkling increases monotonically with R.

This result of our analysis is consistant with the observation of Naziri and Pearce [16] who inferred the effect of R on wrinkling by measuring the blankholder force required to suppress wrinkling. Naziri and Pearce [16] found that the load required to suppress wrinkling generally decreased with increasing R. The results displayed in Table 2 also indicate that if an attempt was made to investigate the effect of R on wrinkling without a blankholder, this effect of the normal anisotropy, R, would not be observed.

Figures 7 through 9 compare the present results with those obtained by Senior [7] employing a beam model of the flange.

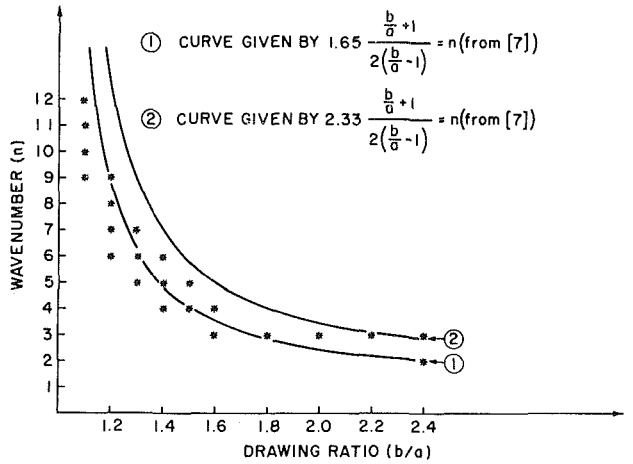

Fig. 7 Critical wavenumber, n, versus the drawing ratio, b/a, for deformation theory and comparison with the results given in [7]. By (*) we denote wavenumbers with critical drawing stresses within $0.01\sigma_y$ of the critical drawing stress. Results obtained for $m = 1, 4, 10$, $h^2/a^2\,\epsilon_y = 0.1, 0.9, 2.5$, $\nu = 0.3$, $R = 1$, $K/h\sigma_y = 0$.

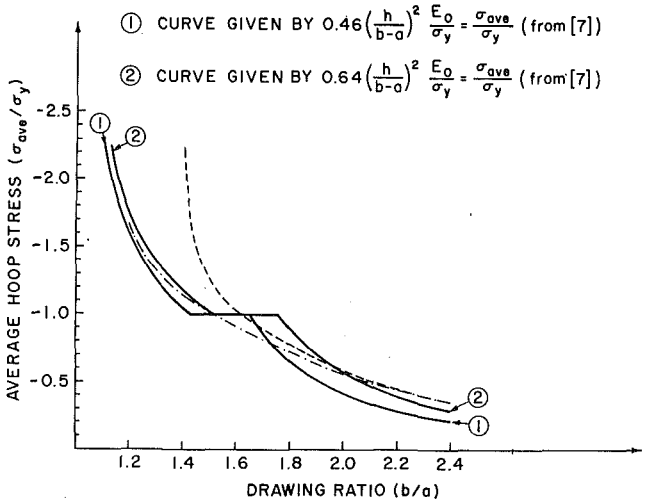

Fig. 8 Average hoop stress at bifurcation, (σ_{ave}/σ_y) versus drawing ratio, b/a, for deformation theory (·····) and flow theory (---) with hardening exponent $m = 4$ and comparison with the results given in [7]. Results obtained for $h^2/a^2 = 0.9$, $\nu = 0.3$, $R = 1$, $K/h\sigma_y = 0$.

Senior's [7] analysis for the onset of wrinkling without a blankholder predicts that the number of wrinkles will lie in the range

$$1.65\,\frac{b/a+1}{2(b/a-1)} \le n \le 2.33\,\frac{b/a+1}{2(b/a-1)} \tag{27}$$

The lower and upper bounds in (27) are plotted in Fig. 7. The points shown in this figure correspond to wavenumbers, n, which are either the critical ones or have critical drawing stresses, $\sigma_{11}^c(a)$, which differ by less than $0.01\sigma_y$ from the critical drawing stress. Senior [7] found that the number of wrinkles observed tended to lie within the range given by (27) or, for smaller drawing ratios, to be somewhat greater than the upper bound in (27). The present results tend to lie slightly below the lower bound. This is most likely due to our idealization of the flange as being simply supported at the die throat, $r = a$. A few calculations were carried out for the extreme case in which the edge $r = a$, is clamped. For a drawing ratio, b/a, of 1.6, $h^2/a^2\epsilon_y = 0.9$ and $m = 4$ with $r = a$ simply supported, the critical drawing stress, $\sigma_{11}^c(a)/\sigma_y$, is 0.55 and the number of wrinkles formed is 4. When $r = a$ is clamped, then $\sigma_{11}^c(a)/\sigma_y = 0.61$ and the critical number of

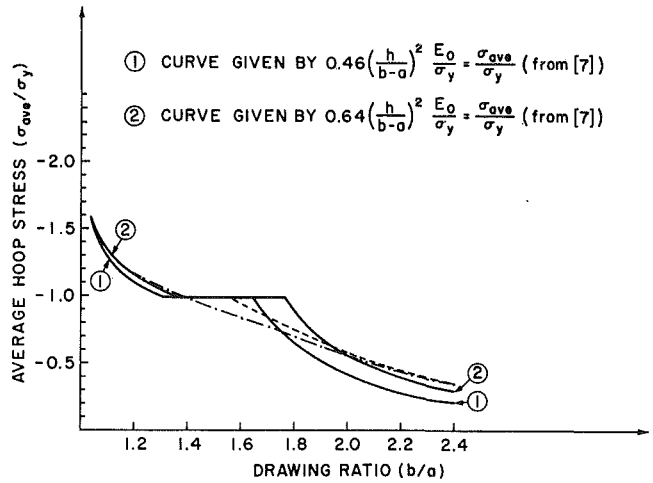

Fig. 9 Average hoop stress at bifurcation (σ_{ave}/σ_y), versus the drawing ratio, b/a, for deformation theory (·····) curves and flow theory (---) with hardening exponent $m = 10$ and comparison with the results given in [7]. Results obtained for $h^2/a\epsilon_y = 0.9$, $\nu = 0.3$, $R - 1$, $K/h\sigma_y = 0$. $K/h\iota$

wrinkles is 6. In the presence of the blankholder this difference is less, with $K/h\sigma_y \simeq 3.5$ for both boundary conditions ($\gamma^{-1}K/h\sigma_y = 100$), $\sigma_{11}^c(a)/\sigma_y = 0.75$, with $n = 9$ and $\sigma_{11}^c(a)/\sigma_y = 0.76$ with $n = 10$, for the simply supported and clamped cases respectively.

Senior's [7] analysis leads to the condition that the onset of wrinkling is bounded by

$$0.46\left(\frac{h}{b-a}\right)^2 \leq \frac{\sigma_{ave}}{E_0} \leq 0.64\left(\frac{h}{b-a}\right)^2 \tag{28}$$

where

$$E_0 = \frac{4EE_t}{(\sqrt{E}+\sqrt{E_t})^2} \tag{29}$$

and σ_{ave} is the average hoop stress in the flange.

In Figs. 8 and 9 the bounds in (28) are compared with the present results. The values of σ_{ave} corresponding to the present results were obtained by numerically integrating the hoop stress, $\sigma_{22}(r)$, from $r = a$ to $r = b$. The discontinuity in the bounds from (28) arises from the discontinuity in E_t at σ_y for the piecewise power hardening model employed in the present analysis, (9). Note that for small drawing ratios the dependence on the drawing ratio given by (28) is qualitiatively like the present results employing the deformation theory. The flow theory results give average hoop stresses at the onset of wrinkling much in excess of (28).

5 Concluding Remarks

The present analysis predicts that the critical drawing stress for the onset of wrinkling is not a monotonic function of the drawing ratio. However, the critical displacement for the onset of wrinkling does increase monotonically as the drawing ratio decreases.

As shown in [15] the limiting drawing ratio (LDR) increases with the plastic anisotropy coefficient R. Here we find that the critical drawing stress and displacement for the onset of wrinkling, with a blankholder present, also increases with R. Results of Senior [7] for the average hoop stress at the onset of wrinkling give a similar qualitative dependence on the drawing ratio to that exhibited by the present results employing deformation theory. However, such a beam model, which employs a uniaxial constitutive law, does not reveal the dependence of the onset of wrinkling on the plastic anisotropy coefficient R.

Naruse and Takeyama [18, 19] also formulate the onset of wrinkling as a plastic bifurcation problem for an annular plate. In [18, 19] attention is confined to the classical smooth yield surface flow theory for an isotropic material and, in [19], a spring type blankholder model differing from that employed here is adopted. Results presented in [18, 19] focus on drawing ratios in the range 1.7 to 2.0 and blankholder stiffnesses, $K/h\sigma_y$, in the range between 0.0 and 1.0.

The present analysis has focussed on the critical conditions governing the onset of wrinkling. Consideration of the rate of growth of wrinkles, or their ironing out, requires a post-bifurcation analysis, which is not undertaken here. Such an analysis is probably most appropriately carried out within the context of a finite deformation formulation.

Acknowledgment

The support of this work by the NSF through Grant ENG76-16421 is gratefully acknowledged. We are indebted to Professor M. Gotoh, Gifu University, visiting at Brown University, for bringing references [18, 19] to our attention as this report was being written.

References

1 *Mechanics of Sheet Metal Forming*, edited by Koistinen, D. P. and Wang, N.-M., Plenum Press, New York, 1978.

2 *Formability: Analysis, Modeling and Experimentation*, edited by Hecker, S. S., Ghosh, A. K. and Gegal, H. L., AIME, New York, 1978.

3 Timoshenko, S. P., and Gere, J. M., *Theory of Elastic Stability*, McGraw-Hill, New York, 1961.

4 Hutchinson, J. W., "Plastic Buckling," *Advances in Applied Mechanics*, edited by C. S. Yih, Vol. 14, 1974, pp. 67–144.

5 Hutchinson, J. W., "Elastic-Plastic Behaviour of Polycrystalline Metals and Composites," *Proceedings of the Royal Society of London*, Vol. A139, 1970, pp. 247–272.

6 Hecker, S. S., "Experimental Studies of Yield Phenomena in Biaxially Loaded Metals," *Constitutive Equations in Viscoplasticity: Computational and Engineering Aspects*, AMD-Vol. 20, ASME, New York, 1976, pp. 1–33.

7 Senior, B. W., "Flange Wrinkling in Deep-Drawing Operations," *Journal of the Mechanics and Physics of Solids*, Vol. 4, 1956, pp. 235–246.

8 Hill, R., *The Mathematical Theory of Plasticity*, Oxford, 1950.

9 Batdorf, S. B., "Theories of Plastic Buckling," *Journal of Aeronautical Sciences*, Vol. 16, 1949, pp. 405–408.

10 Sanders, J. L., "Plastic Stress-Strain Relations Based on Linear Loading Functions," *Proceedings 2nd U. S. National Congress of Applied Mechanics*, 1954, pp. 455–460.

11 Christoffersen, J., and Hutchinson, J. W., "A Class of Phenomenological Corner Theories of Plasticity," *Journal of the Mechanics and Physics of Solids*, Vol. 27, 1979, pp. 465–487.

12 Hill, R., "A General Theory of Uniqueness and Stability in Elastic-Plastic Solids," *Journal of the Mechanics and Physics of Solids*, Vol. 6, 1958, pp. 236–249.

13 Hill, R., "Bifurcation and Uniqueness in Non-Linear Mechanics of Continua," *Problems of Continuum Mechanics*, edited by Lavrent'ev. M. A. et al.; English edition edited by Radok, J. R. M., Society for Industrial and Applied Mathematics, Philadelphia, 1961, pp. 155–164.

14 Needleman, A., "Bifurcation of Elastic-Plastic Spherical Shells Subject to Internal Pressure," *Journal of the Mechanics and Physics of Solids*, Vol. 23, 1975, pp. 257–367.

15 Budiansky, B., and Wang, N.-M., "On the Swift Cup Test," *Journal of the Mechanics and Physics of Solids*, Vol. 14, 1966, pp. 357–374.

16 Naziri, H., and Pearce, R., "The Effect of Plastic Anisotropy on Flange Wrinkling Behaviour During Sheet Metal Forming," *La Metallurgia Italiana*, No. 8, 1968, pp. 727–735.

17 Needleman, A., "Axisymmetric Buckling of Elastic-Plastic Annular Plates," *AIAA Journal*, Vol. 12, 1974, pp. 1594–1596.

18 Naruse, K., and Takeyama, H., "Bifurcation Analysis of a Deep-Drawn Flange without a Blank Holder," (in Japanese with English summary) *Journal of the Japan Society for Technology of Plasticity*, Vol. 18, 1977, pp. 739–745.

19 Naruse, K., and Takeyama, H., "Effects of Restraining Flange Wrinkling by Spring-Type Blank Holder," (in Japanese with English summary) *Journal of the Japan Society for Technology of Plasticity*, Vol. 20, 1979, pp. 386–391.

APPENDIX

For the flow theory of plasticity the three dimensional incremental moduli are given by

$$\hat{L}_{ijkl} = \frac{E}{1+\nu}\left[\frac{1}{2}(\delta_{ik}\delta_{jl}+\delta_{il}\delta_{jk})+\frac{\gamma}{1-2\nu}\delta_{ij}\delta_{kl}-\frac{\dfrac{\partial\sigma_e}{\partial\sigma_{ij}}\cdot\dfrac{\partial\sigma_e}{\partial\sigma_k}}{\dfrac{1+\nu}{\dfrac{E}{E_t}-1}+\dfrac{\partial\sigma_e}{\partial\sigma_{mn}}\cdot\dfrac{\partial\sigma_e}{\partial\sigma_{mn}}}\right] \tag{A1}$$

where σ_e is given by (5).

For the deformation theory

$$L_{ijkl} = \frac{E}{1+\nu}\left[A_{ijkl}+\frac{\nu}{1-2\nu}\delta_{ij}\delta_{kl}-\frac{A_{ijmn}\dfrac{\partial\sigma_e}{\partial\sigma_{mn}}A_{klrs}\dfrac{\partial\sigma_e}{\partial\sigma_{rs}}}{\dfrac{1+\nu}{\dfrac{E}{E_t}-\dfrac{E}{E_s}}+\dfrac{\partial\sigma_e}{\partial\sigma_{mn}}A_{mnrs}\dfrac{\partial\sigma_e}{\partial\sigma_{rs}}}\right] \tag{A2}$$

Here, A_{ijkl} has the symmetries $A_{ijkl} = A_{klij} = A_{jikl} = A_{jilk}$ and satisifies

$$A_{ijkl}\left[\bar{I}_{klmn}+\frac{1}{2}\beta\frac{\partial^2(\sigma^2{}_e)}{\partial\sigma_{kl}\partial\sigma_{mn}}\right]=\left[\bar{I}_{ijkl}+\frac{1}{2}\beta\frac{\partial^2(\sigma^2{}_e)}{\partial\sigma_{ij}\partial\sigma_{kl}}\right]A_{klmn}=\bar{I}_{ijmn} \tag{A3}$$

with $\bar{I}_{ijkl}$ being the fourth order identity, $\bar{I}_{ijkl} = 1/2\ (\delta_{ik}\delta_{jl}+\delta_{il}\delta_{jk})$ and $\beta = (E/E_s-1)/(1+\gamma)$.